

Structure of the $\Lambda(1670)$ resonance

Jiong-Jiong Liu,^{1,2,3} Zhan-Wei Liu^{1,2,3,*} Kan Chen,^{4,5,6,7,8} Dan Guo,⁸ Derek B. Leinweber^{9,†}
Xiang Liu^{1,2,3,‡} and Anthony W. Thomas^{9,§}

¹*School of Physical Science and Technology, Lanzhou University, Lanzhou 730000, China*

²*Research Center for Hadron and CSR Physics, Lanzhou University and Institute of Modern Physics of CAS, Lanzhou 730000, China*

³*Lanzhou Center for Theoretical Physics, Key Laboratory of Theoretical Physics of Gansu Province, Key Laboratory of Quantum Theory and Applications of MoE, and MoE Frontiers Science Center for Rare Isotopes, Lanzhou University, Lanzhou 730000, China*

⁴*School of Physics, Northwest University, Xi'an 710127, China*

⁵*Shaanxi Key Laboratory for theoretical Physics Frontiers, Xi'an 710127, China*

⁶*Institute of Modern Physics, Northwest University, Xi'an 710127, China*

⁷*Peng Huanwu Center for Fundamental Theory, Xi'an 710127, China*

⁸*School of Physics and State Key Laboratory of Nuclear Physics and Technology, Peking University, Beijing 100871, China*

⁹*ARC Special Research Centre for the Subatomic Structure of Matter (CSSM), Department of Physics, University of Adelaide, Adelaide, South Australia 5005, Australia*



(Received 21 December 2023; accepted 26 February 2024; published 18 March 2024)

We examine the internal structure of the $\Lambda(1670)$ through an analysis of lattice QCD simulations and experimental data within Hamiltonian effective field theory. Two scenarios are presented. The first describes the $\Lambda(1670)$ as a bare three-quark basis state, which mixes with the $\pi\Sigma$, $\bar{K}N$, $\eta\Lambda$ and $K\Xi$ meson-baryon channels. In the second scenario, the $\Lambda(1670)$ is dynamically generated from these isospin-0 coupled channels. The K^-p scattering data and the pole structures of the $\Lambda(1405)$ and the $\Lambda(1670)$ can be simultaneously described well in both scenarios. However, a comparison of the finite-volume spectra to lattice QCD calculations reveals significant differences between these scenarios, with a clear preference for the first case. Thus the lattice QCD results play a crucial role in allowing us to distinguish between these two scenarios for the internal structure of the $\Lambda(1670)$.

DOI: [10.1103/PhysRevD.109.054025](https://doi.org/10.1103/PhysRevD.109.054025)

I. INTRODUCTION

Given that the strange quark is considerably heavier than the light quarks, it is a remarkable feature of the baryon spectrum that the lightest odd-parity baryon is not an excited state of the nucleon but lies within the Λ family, with nonzero strangeness. This resonance, the $\Lambda(1405)$, with $I(J^P) = 0(1/2^-)$, has been the subject of considerable theoretical work and speculation. Before the discovery of quarks, Dalitz and Tuan suggested that it might

be a $\bar{K}N$ molecule, since its mass is slightly below the $\bar{K}N$ threshold [1]. However, there have been many other options explored since then, including conventional baryon states, dynamically generated states, three-quark states mixing with multi-quark components as well as other explanations [2–33].

In the first study based upon SU(3) chiral symmetry after the discovery of QCD, Veit *et al.* also concluded that their result “strongly support[ed] the contention that the $\Lambda(1405)$ is a $\bar{K}N$ bound state” [34]. This interpretation has also been supported by studies within the chiral unitary approach [3,4,35], as well as in an analysis of lattice QCD data by the CSSM group [36–38] using Hamiltonian effective field theory (HEFT) [39–44].

There has been considerable interest in the analytic structure of the S-matrix for this system. In particular, the two-pole structure of the $\Lambda(1405)$, once SU(3) chiral symmetry of QCD was treated seriously, was unveiled for the first time in Ref. [4]. The two resonance poles in the second Riemann sheet are related to the thresholds of the $\bar{K}N$ and $\pi\Sigma$ channels [37,45–49]. The evolution of the

*liuzhanwei@lzu.edu.cn

†derek.leinweber@adelaide.edu.au

‡xiangliu@lzu.edu.cn

§anthony.thomas@adelaide.edu.au

Published by the American Physical Society under the terms of the [Creative Commons Attribution 4.0 International license](https://creativecommons.org/licenses/by/4.0/). Further distribution of this work must maintain attribution to the author(s) and the published article's title, journal citation, and DOI. Funded by SCOAP³.

poles for the $\Lambda(1380)$, $\Lambda(1405)$ and $\Lambda(1670)$ away from the SU(3) limit was first studied in Ref. [3].

There have recently been many other examples of systems which are suspected of being molecular in nature. For example, this has been proposed [50,51] as an explanation of the $\Xi(1620)$ recently observed by the Belle collaboration [52]. When it comes to heavy quarks, many multi-quark states have been announced by different experiments, including the $P_c(4312)$, $P_c(4440)$, $P_c(4457)$ [53,54], $T_{cc}(3875)$ [55,56], $P_{cs}(4459)$ [57], and the $P_{cs}(4338)$ [58]. The occurrence of these exotic states near thresholds and their exotic quark content has resulted in the molecular picture being a popular interpretation of these states.

As the $\Lambda(1405)$ is now commonly interpreted as a $\bar{K}N$ bound state, it is natural to ask where one might find the lightest P -wave uds baryon expected in the conventional quark model. The analysis of Veit *et al.* suggested that the $J^P = 1/2^-$ $\Lambda(1670)$ might be identified with this triquark core [34]. In such a scenario the structure of the $\Lambda(1405)$ and the $\Lambda(1670)$ would be very different. It is important to investigate this interpretation very carefully, given the suggestion that once one removes molecular-like states from the baryon spectrum it appears as though the quark model idea of oscillator-like major shells might be correct [59].

With this in mind, here we present a detailed study of the $S = -1$, $J^P = \frac{1}{2}^-$ system, covering both the $\Lambda(1670)$ and the $\Lambda(1405)$ resonance region within HEFT. First we extend our earlier analysis of the cross section data for K^-p scattering to include K^- laboratory momenta up to 800 MeV/c, including the near threshold cross sections measured in 2022 [60]. The pole structure of the $\Lambda(1670)$ and the $\Lambda(1405)$ resonances are examined.

We analyze the lattice QCD data for the negative parity Λ baryons [16,31,38,61], as well as the corresponding eigenvectors describing the structure of those eigenstates. Given that just a few months ago, the BaSc collaboration presented their coupled-channel simulations with both single baryon and meson-baryon interpolating operators at $m_\pi \approx 200$ MeV, which is close to the physical pion mass [62,63], we pay particular attention to their results [62,63].

On the experimental side, there has been considerable progress in updating the K^-p scattering information associated with the negative-parity Λ baryons, which has been included in our analysis. For example, J-PARC provided the $\pi\Sigma$ invariant mass spectra in K^-p induced reactions on the deuteron in 2022 [64]. The ALICE collaboration extracted the K^-p scattering length with a measurement of momentum correlations in 2021 [65], while measurements of the energy shift of the 1s-state in kaonic-hydrogen by the SIDDHARTA collaboration have yielded precise values for the K^-p scattering lengths [66,67]. Simultaneous $K^-p \rightarrow \Sigma^0\pi^0, \Lambda\pi^0$ near-threshold cross sections were measured at DAΦNE in 2022 [60].

This paper is organized as follows. In Sec. II, we outline the HEFT framework as applied to the negative parity Λ hyperons, while in Sec. IV the corresponding numerical results and discussion are presented. A summary and concluding remarks are provided in Sec. V.

II. HAMILTONIAN EFFECTIVE FIELD THEORY

In this section, we introduce the framework within which we describe the K^-p scattering processes. In order to obtain the mass spectra of Λ baryons with $J^P = 1/2^-$, which can be compared with those observed in lattice QCD, we also present the finite-volume Hamiltonian.

A. The Hamiltonian

In the rest frame, the Hamiltonian includes noninteracting and interacting parts

$$H^I = H_0^I + H_{\text{int}}^I, \quad (2.1)$$

where the kinetic energy piece of the Hamiltonian is written as

$$H_0^I = \sum_{B_0} |B_0\rangle m_B^0 \langle B_0| + \sum_{\alpha} \int d^3k |\alpha(k)\rangle [\omega_{\alpha_M}(k) + \omega_{\alpha_B}(k)] \langle \alpha(k)|. \quad (2.2)$$

Here, B_0 denotes a ‘‘bare baryon’’ with mass m_B^0 . This state may be interpreted as representing a quark model baryon, which is then dressed by its coupling to meson-baryon channels [68]. Here α labels the meson-baryon channel and α_M (α_B) is the meson (baryon) in channel α . The meson (baryon) energy is simply

$$\omega_{\alpha_{M(B)}}(k) = \sqrt{m_{\alpha_{M(B)}}^2 + k^2}. \quad (2.3)$$

For the interacting part of the Hamiltonian we include a vertex interaction coupling the bare baryon to the meson-baryon channel α

$$g^I = \sum_{B_0, \alpha} \int d^3k \{ |B_0\rangle G_{B_0, \alpha}^{I\dagger}(k) \langle \alpha(k)| + \text{H.c.} \}, \quad (2.4)$$

as well as the direct two-to-two particle interactions

$$v^I = \sum_{\alpha, \beta} \int d^3k d^3k' |\alpha(k)\rangle V_{\alpha, \beta}^I(k, k') \langle \beta(k')|. \quad (2.5)$$

The form factors associated with the coupling of the bare baryon to meson-baryon channel α are

$$G_{B_0, \alpha}^I(k) = \frac{\sqrt{3} g_{B_0, \alpha}^I}{2\pi f} \sqrt{\omega_{\alpha_M}(k)} u(k), \quad (2.6)$$

and the form of the potentials motivated by the Weinberg-Tomozawa interaction [34,69,70] are

$$V_{\alpha,\beta}^I(k, k') = g_{\alpha,\beta}^I \frac{[\omega_{\alpha_M}(k) + \omega_{\beta_B}(k')]u(k)u(k')}{8\pi^2 f^2 \sqrt{2\omega_{\alpha_M}(k)}\sqrt{2\omega_{\beta_B}(k')}}. \quad (2.7)$$

Here, we use the dipole form factor $u(k) = (1 + k^2/\Lambda^2)^{-2}$ with regulator parameter $\Lambda = 1$ GeV. The $g_{B_0,\alpha}^I$ and $g_{\alpha,\beta}^I$ are the couplings of the corresponding interaction terms in the isospin I channel. As discussed in Sec. III.C of Ref. [71], when working in a nonperturbative effective field theory, couplings encounter significant renormalization such that the perturbative couplings are best promoted to fit parameters. While this is a form of modeling, the Lüscher formalism within HEFT protects the model-independent relation between the scattering observables and the finite-volume spectrum. As discussed in Sec. III, our task is to ensure there are sufficient parameters to accurately describe the scattering data.

B. Infinite-volume scattering amplitude

Here we introduce the formalism to describe the cross sections of K^-p scattering in infinite volume. The two particle scattering T matrices can be obtained by the three-dimensional reduction of the coupled-channel Bethe-Salpeter equation

$$T_{\alpha,\beta}^I(k, k'; E) = \tilde{V}_{\alpha,\beta}^I(k, k'; E) + \sum_{\gamma} \int q^2 dq \frac{\tilde{V}_{\alpha,\gamma}^I(k, q; E) T_{\gamma,\beta}^I(q, k'; E)}{E - \omega_{\gamma_1}(q) - \omega_{\gamma_2}(q) + i\epsilon}, \quad (2.8)$$

where the scattering potential can be expressed from the interaction Hamiltonian above

$$\tilde{V}_{\alpha,\beta}^I(k, k'; E) = \sum_{B_0} \frac{G_{B_0,\alpha}^{I\dagger}(k) G_{B_0,\beta}^I(k')}{E - m_{B_0}^0} + V_{\alpha,\beta}^I(k, k'). \quad (2.9)$$

Note that for K^-p scattering the T matrices, $t_{\alpha,\beta}(k, k'; E)$, appear as a linear combination of $I = 0$ and $I = 1$ channels, i.e., $T_{\alpha,\beta}(k, k'; E) = aT_{\alpha,\beta}^{I=0}(k, k'; E) + bT_{\alpha,\beta}^{I=1}(k, k'; E)$, where a and b involve the corresponding Clebsch-Gordan coefficients. The poles associated with the $\Lambda(1405)$ and $\Lambda(1670)$ can be obtained by searching for those of the $T_{\alpha,\beta}^{I=0}(k, k'; E_{\text{pole}})$ matrix on the unphysical Riemann sheet.

In addition, the cross section for the process $\beta \rightarrow \alpha$ is related to the T matrices by

$$\sigma_{\alpha,\beta} = \frac{4\pi^3 k_{\text{acm}} \omega_{\alpha_M \text{cm}} \omega_{\alpha_B \text{cm}} \omega_{\beta_M \text{cm}} \omega_{\beta_B \text{cm}}}{E_{\text{cm}}^2 k_{\beta \text{cm}}} \times |T_{\alpha,\beta}(k_{\text{acm}}, k_{\beta \text{cm}}; E_{\text{cm}})|^2, \quad (2.10)$$

where the subscript ‘‘cm’’ refers to the center-of-mass momentum frame.

C. Finite-volume Hamiltonian model

The scattering processes need interactions in both the $I = 0$ and $I = 1$ channels. Since the mass of $\Lambda(1670)$ is only 130 MeV below the $K\Xi$ threshold, in this work we include the $K\Xi$ as well as the $\pi\Sigma$, $\bar{K}N$, and $\eta\Lambda$ channels for $I = 0$ and the $\pi\Sigma$, $\bar{K}N$, $\pi\Lambda$, $\eta\Sigma$, and $K\Xi$ channels for $I = 1$. In the finite volume, the Hamiltonian \mathcal{H} consists of free and interacting terms, $\mathcal{H} = \mathcal{H}_0 + \mathcal{H}_I$. Such a Hamiltonian can be expressed as a matrix, using the corresponding discrete momentum basis.

In the cubic, finite volume of lattice QCD with length L , the momentum of a particle is $k_n = 2\pi\sqrt{n}/L$, with $n = n_x^2 + n_y^2 + n_z^2$, where $n = 0, 1, 2, \dots$. The noninteracting isospin-0 Hamiltonian is

$$\mathcal{H}_0^0 = \text{diag}\{m_B^0, \omega_{\pi\Sigma}(k_0), \omega_{\bar{K}N}(k_0), \omega_{\eta\Lambda}(k_0), \omega_{K\Xi}(k_0), \dots, \omega_{\pi\Sigma}(k_1), \dots\} \quad (2.11)$$

and the interacting Hamiltonian can be written as

$$\mathcal{H}_{\text{int}}^0 = \begin{pmatrix} 0 & \mathcal{G}_{B_0,\pi\Sigma}^0(k_0) & \mathcal{G}_{B_0,\bar{K}N}^0(k_0) & \mathcal{G}_{B_0,\eta\Lambda}^0(k_0) & \mathcal{G}_{B_0,K\Xi}^0(k_0) & \mathcal{G}_{B_0,\pi\Sigma}^0(k_1) & \dots \\ \mathcal{G}_{B_0,\pi\Sigma}^0(k_0) & \mathcal{V}_{\pi\Sigma,\pi\Sigma}^0(k_0, k_0) & \mathcal{V}_{\pi\Sigma,\bar{K}N}^0(k_0, k_0) & \mathcal{V}_{\pi\Sigma,\eta\Lambda}^0(k_0, k_0) & \mathcal{V}_{\pi\Sigma,K\Xi}^0(k_0, k_0) & \mathcal{V}_{\pi\Sigma,\pi\Sigma}^0(k_0, k_1) & \dots \\ \mathcal{G}_{B_0,\bar{K}N}^0(k_0) & \mathcal{V}_{\bar{K}N,\pi\Sigma}^0(k_0, k_0) & \mathcal{V}_{\bar{K}N,\bar{K}N}^0(k_0, k_0) & \mathcal{V}_{\bar{K}N,\eta\Lambda}^0(k_0, k_0) & \mathcal{V}_{\bar{K}N,K\Xi}^0(k_0, k_0) & \mathcal{V}_{\bar{K}N,\pi\Sigma}^0(k_0, k_1) & \dots \\ \mathcal{G}_{B_0,\eta\Lambda}^0(k_0) & \mathcal{V}_{\eta\Lambda,\pi\Sigma}^0(k_0, k_0) & \mathcal{V}_{\eta\Lambda,\bar{K}N}^0(k_0, k_0) & \mathcal{V}_{\eta\Lambda,\eta\Lambda}^0(k_0, k_0) & \mathcal{V}_{\eta\Lambda,K\Xi}^0(k_0, k_0) & \mathcal{V}_{\eta\Lambda,\pi\Sigma}^0(k_0, k_1) & \dots \\ \mathcal{G}_{B_0,K\Xi}^0(k_0) & \mathcal{V}_{K\Xi,\pi\Sigma}^0(k_0, k_0) & \mathcal{V}_{K\Xi,\bar{K}N}^0(k_0, k_0) & \mathcal{V}_{K\Xi,\eta\Lambda}^0(k_0, k_0) & \mathcal{V}_{K\Xi,K\Xi}^0(k_0, k_0) & \mathcal{V}_{K\Xi,\pi\Sigma}^0(k_0, k_1) & \dots \\ \mathcal{G}_{B_0,\pi\Sigma}^0(k_1) & \mathcal{V}_{\pi\Sigma,\pi\Sigma}^0(k_1, k_0) & \mathcal{V}_{\pi\Sigma,\bar{K}N}^0(k_1, k_0) & \mathcal{V}_{\pi\Sigma,\eta\Lambda}^0(k_1, k_0) & \mathcal{V}_{\pi\Sigma,K\Xi}^0(k_1, k_0) & \mathcal{V}_{\pi\Sigma,\pi\Sigma}^0(k_1, k_1) & \dots \\ \vdots & \vdots & \vdots & \vdots & \vdots & \vdots & \ddots \end{pmatrix}, \quad (2.12)$$

where

$$\mathcal{G}_{B_0,\alpha}^0 = \sqrt{\frac{C_3(n)}{4\pi}} \left(\frac{2\pi}{L}\right)^{3/2} G_{B_0,\alpha}^0(k_n), \quad (2.13)$$

$$\mathcal{V}_{\alpha,\beta}^0(k_n, k_m) = \frac{\sqrt{C_3(n)C_3(m)}}{4\pi} \left(\frac{2\pi}{L}\right)^3 V_{\alpha,\beta}^0(k_n, k_m). \quad (2.14)$$

Here, $C_3(n)$ denotes the number of ways one can sum the squares of three integers to equal n .

III. MODEL (IN)DEPENDENCE IN HEFT

Understanding the model-dependent and model-independent aspects of HEFT is important. HEFT incorporates the Lüscher formalism [39,42], and therefore there are aspects of the calculation that share the same level of model independence as the Lüscher formalism itself.

A. Model independence

The Lüscher formalism provides a rigorous relationship between the finite-volume energy spectrum and the scattering amplitudes of infinite-volume experiment. In HEFT, this relationship is mediated by a Hamiltonian. In the traditional approach, the parameters of the Hamiltonian are tuned to describe lattice QCD results. When the fit provides a high-quality description of lattice QCD results, the associated scattering-amplitude predictions are of high quality. The key is to have a sufficient number of tunable parameters within the Hamiltonian to accurately describe the lattice QCD results.

However, in the baryon sector, high-quality lattice QCD results are scarce and HEFT is usually fit to experimental data first. The HEFT formalism then describes the finite-volume dependence of the baryon spectrum, indicating where high-precision lattice QCD results will reside. This is the approach adopted herein. We will show high-quality fits to the experimental scattering observables such that HEFT provides rigorous predictions of the finite-volume lattice QCD spectrum with model independence at the level of the Lüscher formalism.

Of course, this model independence is restricted to the case of matched quark masses in finite-volume and infinite-volume. The Lüscher formalism provides no avenue for changing the quark mass. In other words, direct contact with lattice QCD results is only possible when the quark masses used in the lattice QCD simulations are physical.

On the other hand, χ PT is renowned for describing the quark mass dependence of hadron properties in a model-independent manner, provided one employs the truncated expansion in the power-counting regime, where higher-order terms not considered in the expansion are small by definition. Given that finite-volume HEFT reproduces the leading behavior of finite-volume χ PT in the perturbative limit by construction [42,71], it is reasonable to explore the

extent to which this model independence persists in the full nonperturbative calculation of HEFT.

This has been explored in Ref. [71]. In the one-channel case where a single particle basis state (e.g. a quark-model like Δ) couples to one two-particle channel (e.g. πN), the independence of the results on the form of regularization is reminiscent of that realized in χ PT. Any change in the regulator is absorbed by the low-energy coefficients such that the renormalized coefficients are physical, independent of the renormalization scheme.

However, in the more complicated two-channel case with a $\pi\Delta$ channel added, the same was not observed. The form of the Hamiltonian becomes constrained, describing experimental data accurately for only a limited range of parameters with specific regulator shapes. The Hamiltonian becomes a model in this case, with regulator-function scales and shapes governed by the experimental data. The principles of chiral *perturbation* theory no longer apply in this nonperturbative calculation. However, for fit parameters that describe the data well, the model independence of the Lüscher formalism remains intact. The Hamiltonian is only a intermediary.

B. Quark mass variation

The consideration of variation of the quark masses away from the physical point provides further constraints on the Hamiltonian. In particular, lattice QCD results away from the physical point provide new constraints on the form of the Hamiltonian. In the two-channel case, the Hamiltonian becomes tightly constrained when considering experimental scattering data and lattice QCD results together [71].

With the Hamiltonian determined by one set of lattice results, one can then make predictions of the finite-volume spectrum considered by other lattice groups at different volumes and different quark masses. This is a central aim of the current investigation where we confront very recent lattice QCD predictions for the odd-parity Λ spectrum at an unphysical pion mass of 204 MeV [62,63]. The Hamiltonian will be constrained by lattice QCD results from Refs. [31,38] for the lowest-lying odd-parity excitation, such that the confrontation with contemporary lattice QCD results is predictive.

For the cases previously considered in the baryon spectrum the predictions of HEFT are in agreement with lattice QCD spectrum predictions. For example, in the Δ -channel, HEFT successfully predicts the finite-volume spectrum of the CLS consortium [71,72]. In the $N1/2^+$ channel, HEFT reproduces the lattice QCD results from Lang *et al.* [59,73]. In the $N1/2^-$ channel, HEFT successfully predicts spectra from the CLS consortium [41,74], the HSC [41,75,76] and Lang and Verducci [41,77]. Thus one concludes that the systematic errors of the HEFT approach to quark-mass variation are small on the scale of contemporary lattice QCD uncertainties. As the Hamiltonian is constrained by model-independent scattering data and

lattice QCD results, we expect this success to be realized in the current investigation.

Variation in the quark mass is conducted in the same spirit as for χ PT. The couplings are held constant and the hadron masses participating in the theory take values as determined in lattice QCD. The single-particle bare basis state acquires a quark mass dependence and this is done in the usual fashion by drawing on terms analytic in the quark mass. In most cases, lattice QCD results are only able to constrain a term linear in m_π^2 , as is the case here.

The model independence associated with the movement of quark masses away from the physical point is largely governed by the distance one chooses to move from the physical quark-mass point. The HEFT approach is systematically improvable, reliant on high-quality lattice QCD results to constrain the higher-order terms that one can introduce. For example, one could include an additional analytic m_π^4 term or higher-order interaction terms from the chiral Lagrangian. However, this increased level of precision is not yet demanded by current experimental measurements nor contemporary lattice QCD results.

C. Model dependence

Now that the Hamiltonian has become a tightly constrained model, the eigenvectors describing the manner in which the noninteracting basis states come together to compose the eigenstates of the spectrum are model dependent. At the same time, there is little freedom in the model parameters of the Hamiltonian such that the predictions of the Hamiltonian are well defined.

The information contained in the Hamiltonian eigenvectors describing the basis-state composition of finite-volume energy eigenstates is analogous to the information contained within the eigenvectors of lattice QCD correlation matrices describing the linear combination of interpolating fields isolating energy eigenstates on the lattice. These too are model dependent, governed by the nature of the interpolating fields used to construct the correlation matrix.

What is remarkable is that with a suitable renormalization scheme on the lattice (e.g. interpolators are normalized to set diagonal correlators equal to 1 at one time slice after the source), the composition of the states drawn from the lattice correlation matrix is very similar to the description provided by HEFT [41,59]. While both eigenvector sets are model dependent, their similarity does indeed provide some relevant insight into hadron structure. And because regularization in the Hamiltonian is tightly constrained, one can begin to separate out the contributions of bare versus two-particle channels.

D. Error analysis

It may be of interest to compare the systematic uncertainties of the HEFT formalism with the statistical uncertainties of contemporary lattice QCD determinations of the

finite-volume hadron spectrum. To do so requires an exploration of alternative Hamiltonians that continue to describe both experimental data and lattice QCD results.

Variation of the regularization parameters provides an opportunity to move in the Hamiltonian parameter space. However, the constraints of experiment and lattice QCD are quite effective in constraining the Hamiltonian, allowing only a small range of variation in the regularization parameters. Moving the parameters outside of the range allowed by the data, spoils the fit to the data and thus the associated finite-volume energy spectrum.

Recalling that the embedded Lüscher formalism governs the relation between the scattering data and the finite-volume spectrum and noting that the Hamiltonian plays only a mediary role, one concludes that the systematic error is governed by the quality of the experimental data and its ability to uniquely constrain the multichannel Hamiltonian. This issue is quantified in the following section.

E. Summary

In summary, there is a direct model-independent link between the scattering observables of experiment and the finite-volume spectrum calculated in HEFT at physical quark masses. This model independence is founded on the Lüscher formalism embedded with HEFT. Similarly, variation of the quark masses away from the physical quark mass has systematic uncertainties that are small relative to contemporary lattice QCD spectral uncertainties. Finally, the Hamiltonian eigenvectors describing the basis-state composition of finite-volume energy eigenstates are model dependent. They are analogous to the interpolator dependent eigenvectors of lattice QCD correlation matrices describing the linear combination of interpolating fields isolating energy eigenstates on the lattice. The similarity displayed by these two different sets of eigenvectors suggests that they do indeed provide insight into hadron structure.

IV. NUMERICAL RESULTS

In this section, we first study the K^-p cross section, adjusting the parameters of the interaction Hamiltonian to reproduce the experimental data. Then we use these fitted parameters to discuss the finite-volume results.

A. Cross section

As the internal structure of the $\Lambda(1670)$ is still not very clear, we examine two possible scenarios. In the first, we postulate that the $\Lambda(1670)$ is a resonance which is dynamically generated through rescattering in the isospin- $0\pi\Sigma$, $\bar{K}N$, $\eta\Lambda$ and $K\Xi$ coupled channels. In the second, the $\Lambda(1670)$ is treated as a quark-model-like baryon, which mixes with the meson-baryon channels. We fit the experimental data for the $K^-p \rightarrow K^-p$, $K^-p \rightarrow \bar{K}^0n$, $K^-p \rightarrow \pi^0\Lambda^0$, $K^-p \rightarrow \pi^-\Sigma^+$, $K^-p \rightarrow \pi^0\Sigma^0$, $K^-p \rightarrow \pi^+\Sigma^-$, and

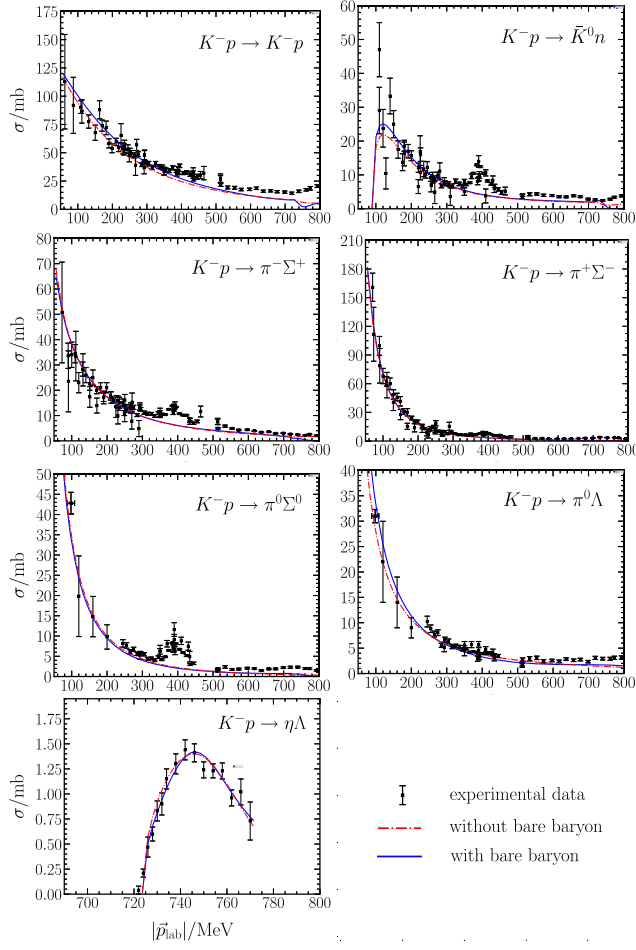


FIG. 1. Experimental data [60,78–90] for the cross sections of $K^-p \rightarrow K^-p$, \bar{K}^0n , $\pi^-\Sigma^+$, $\pi^0\Sigma^0$, $\pi^+\Sigma^-$, and $\eta\Lambda$ scattering processes. The blue solid lines denote the fit including a bare quark-model-like basis state, while the red dashed lines denote the fit without including a bare-baryon component. The peaks around 400 MeV are associated with the D -wave $\Lambda(1520)$ state which is not considered in this work as described in the text.

$K^-p \rightarrow \eta\Lambda$ cross sections over the laboratory momentum range 0–800 MeV, which covers both resonances. We will explore which scenario can give a better description to the experimental cross section data.

We present a comparison of the experimental cross sections with our fitted results in Fig. 1. The fitted parameters are given in Table I. The peak of $\Lambda(1670)$ can be clearly seen in the $K^-p \rightarrow \eta\Lambda$ channel shown in the last subfigure of Fig. 1. It is clear that we can describe this resonance well, both with and without the bare quark-model-like baryon.

From Fig. 1, we see that the calculated cross section and the experimental cross section data have clear discrepancies at laboratory momenta $\vec{p}_{\text{lab}} = 350\text{--}450$ MeV in the $K^-p \rightarrow \bar{K}^0n$, $\pi^-\Sigma^+$, and $\pi^0\Sigma^0$ processes. Here, we need to emphasize that we only introduce the S -wave interactions relevant to spin-1/2 odd-parity Λ baryons. It is well

TABLE I. The fit parameters obtained from K^-p cross sections within the following two scenarios. One describes the $\Lambda(1670)$ as a bare quark-model-like single-particle state mixed with meson-baryon interactions from the $\pi\Sigma$, $\bar{K}N$, $\eta\Lambda$, and $K\Xi$ channels. The other describes the $\Lambda(1670)$ as pure dynamically-generated resonance from isoscalar coupled channels. Error estimates for the bare baryon case are obtained through the consideration of allowed variation in the regularization parameter, Λ , as described in Sec IV C.

Coupling	Without bare baryon	With bare baryon
Λ (GeV)	1.0	$1.0^{+0.1}_{-0.1}$
$g_{\bar{K}N,\bar{K}N}^0$	-2.108	$-2.180^{+0.280}_{-0.135}$
$g_{\bar{K}N,\pi\Sigma}^0$	0.837	$0.620^{-0.076}_{+0.080}$
$g_{\bar{K}N,\eta\Lambda}^0$	-0.461	$-0.472^{+0.471}_{-0.864}$
$g_{\pi\Sigma,\pi\Sigma}^0$	-1.728	$-1.200^{-0.078}_{-0.116}$
$g_{\pi\Sigma,K\Xi}^0$	-0.001	$-1.800^{+0.452}_{-0.200}$
$g_{\eta\Lambda,K\Xi}^0$	0.835	$1.993^{-0.668}_{-0.047}$
$g_{K\Xi,K\Xi}^0$	-3.393	$-1.000^{-0.001}_{-2.314}$
$g_{\bar{K}N,\bar{K}N}^1$	-0.028	$-0.001^{+0.000}_{+0.000}$
$g_{\bar{K}N,\pi\Sigma}^1$	0.829	$0.985^{-0.152}_{+0.268}$
$g_{\bar{K}N,\pi\Lambda}^1$	0.001	$0.990^{-0.108}_{+0.154}$
$g_{\bar{K}N,\eta\Sigma}^1$	1.557	$1.500^{-0.212}_{+0.215}$
$g_{\pi\Sigma,\pi\Sigma}^1$	-1.351	$-0.001^{-0.001}_{+0.000}$
$g_{\pi\Sigma,K\Xi}^1$	-1.017	$-1.341^{+0.197}_{-0.439}$
$g_{\pi\Lambda,K\Xi}^1$	2.904	$0.011^{-0.010}_{-0.010}$
$g_{\eta\Sigma,K\Xi}^1$	4.690	$0.001^{+0.000}_{+0.000}$
$g_{K\Xi,K\Xi}^1$	-0.447	$-3.700^{+0.660}_{-0.840}$
$g_{B_0,\bar{K}N}^0$...	$0.091^{-0.014}_{+0.032}$
$g_{B_0,\pi\Sigma}^0$...	$0.049^{+0.002}_{+0.001}$
$g_{B_0,\eta\Lambda}^0$...	$-0.164^{-0.010}_{+0.014}$
$g_{B_0,K\Xi}^0$...	$-0.226^{-0.005}_{+0.079}$
m_B^0 (MeV)	...	1750^{+39}_{-29}
Pole 1 (MeV)	$1336 - 87i$	$1324^{-4}_{-4} - 67^{+8}_{+10}i$
Pole 2 (MeV)	$1430 - 26i$	$1428^{+4}_{+2} - 24^{+4}_{+0}i$
Pole 3 (MeV)	$1676 - 17i$	$1674^{+2}_{-4} - 11^{+4}_{+3}i$

known (e.g., Refs. [91,92]) that such discrepancies can be well understood by introducing the effects from P and D waves, while the S -wave interactions play essentially no role in forming those peaks. Specifically, Refs. [92–94] presented detailed analyses showing that the peaks at $p_{\text{lab}} = 350\text{--}450$ MeV in $K^-p \rightarrow \pi^0\Sigma^0$ and $\pi^\pm\Sigma^\mp$ arise mainly from contributions involving the D -wave $\Lambda(1520)$ state. The contribution from the $\Lambda(1520)$ is also responsible for the peak in the energy range $\vec{p}_{\text{lab}} = 350\text{--}450$ MeV in the $K^-p \rightarrow \bar{K}^0n$ process [93]. Because they have different quantum numbers, these contributions

cannot influence the $\Lambda(1670)$, and we do not consider them further.

In the channels of $K^-p \rightarrow K^-p$, $K^-p \rightarrow \bar{K}^0n$, $K^-p \rightarrow \pi^0\Lambda^0$, and $K^-p \rightarrow \pi^0\Sigma^0$, the cross sections for $\vec{p}_{\text{lab}} > 500$ MeV are much smaller than those at LOW momenta. The $\Lambda(1670)$ resonance is not obvious in these channels either. Since we do not consider further channels, such as \bar{K}^*N and $\pi\Sigma^*$, which are close to this energy region, our results deviate from the experimental data for $\vec{p}_{\text{lab}} > 500$ MeV in some channels.

Except for these minor discrepancies, our calculations in both scenarios give a very good description of the experimental data. The recently measured threshold cross sections in Ref. [60] for $K^-p \rightarrow \pi^0\Lambda^0$, and $K^-p \rightarrow \pi^0\Sigma^0$ provide more accurate constraints and can be described well, as can be seen in the third row of Fig. 1. The line shapes of the fits with and without the inclusion of a bare-baryon contribution are very similar.

Using these fits, we can obtain the $\Lambda(1670)$ pole in both scenarios. As shown in Table I, in the first scenario the pole position is located at $1676 - 17i$ MeV. This is not far from that in the second scenario, namely $1674 - 11i$ MeV. Our results are consistent with those of other groups [5,22–24,26,95–97]. The well-known two-pole structure of the $\Lambda(1405)$ is also reproduced.

The close agreement between the two scenarios for the fitted cross sections, as well as the pole positions, indicate that the present experimental data are not able to distinguish between these two very different physical pictures for the structure of the $\Lambda(1670)$. Therefore, we bring these results to the finite volume of lattice QCD and confront their predictions with lattice QCD simulation results.

B. Finite volume spectrum and structure

As discussed in the previous subsection, the scenarios with or without a bare basis state give very similar fits to contemporary experimental cross section data. That is, the present experimental data are not able to distinguish the internal structure. We shall see that the lattice QCD simulation results provide more information about this question.

By studying the finite-volume Hamiltonian with the fitted parameters given in Table I, we can obtain the corresponding lattice energy eigenvalues and eigenvectors. The lattice QCD results are provided at different pion masses, and thus we need the hadron mass dependence on the pion mass as input. For the masses of $m_K(m_\pi^2)$, $m_N(m_\pi^2)$, $m_\Lambda(m_\pi^2)$, $m_\Sigma(m_\pi^2)$, and $m_\Xi(m_\pi^2)$, we use a smooth interpolation of the corresponding lattice QCD results. The mass of the η meson is [98]

$$m_\eta(m_\pi^2) = \sqrt{m_\eta^2|_{\text{phy}} + \frac{1}{3}(m_\pi^2 - m_\pi^2|_{\text{phy}})}. \quad (4.1)$$

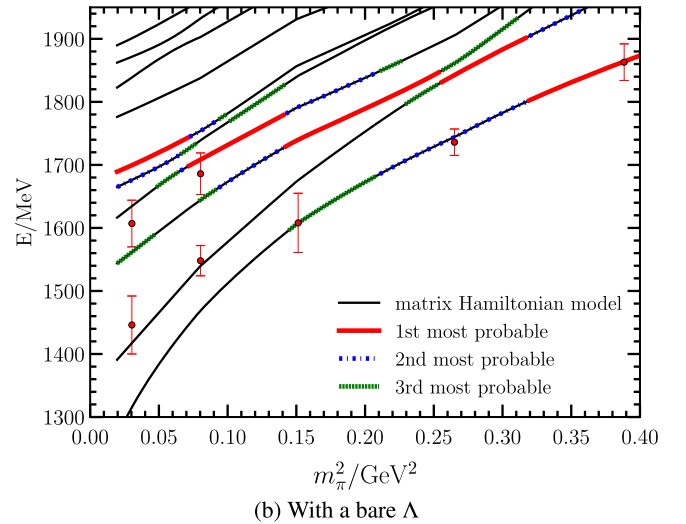
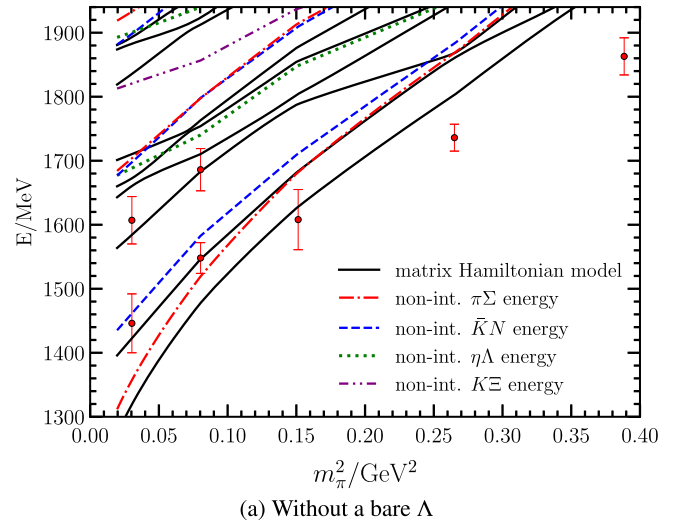


FIG. 2. The pion mass dependence of the eigenstates obtained using the finite-volume Hamiltonian. In the upper plot, the broken lines denote noninteracting meson-baryon energies, while the solid lines denote the eigenenergies obtained from the finite-volume Hamiltonian matrix. In the lower plot, energy eigenstates based on the inclusion of a bare quark-model-like basis state are illustrated. The thick (red), dot-dashed (blue), and dotted (green) lines label the states composed with a significant contribution from the bare quark-model-like basis state, with red illustrating the largest bare state component. The negligible component of the bare basis state in the first state of the spectrum at light quark masses explains its absence in the lattice QCD spectrum excited with local three-quark operators. The lattice results are taken from the CSSM group [31,38] in 2 + 1 flavor QCD [99].

We plot the pion mass dependence of the eigenstates in the finite volume Hamiltonian in Fig. 2(a) for the case where the $\Lambda(1670)$ is a state without a bare baryon component. The lattice results in ~ 3 fm box, shown as red dots with error bar, are taken from the CSSM group [31,38] in 2 + 1 flavor QCD [99]. From Fig. 2(a), we find that the results are

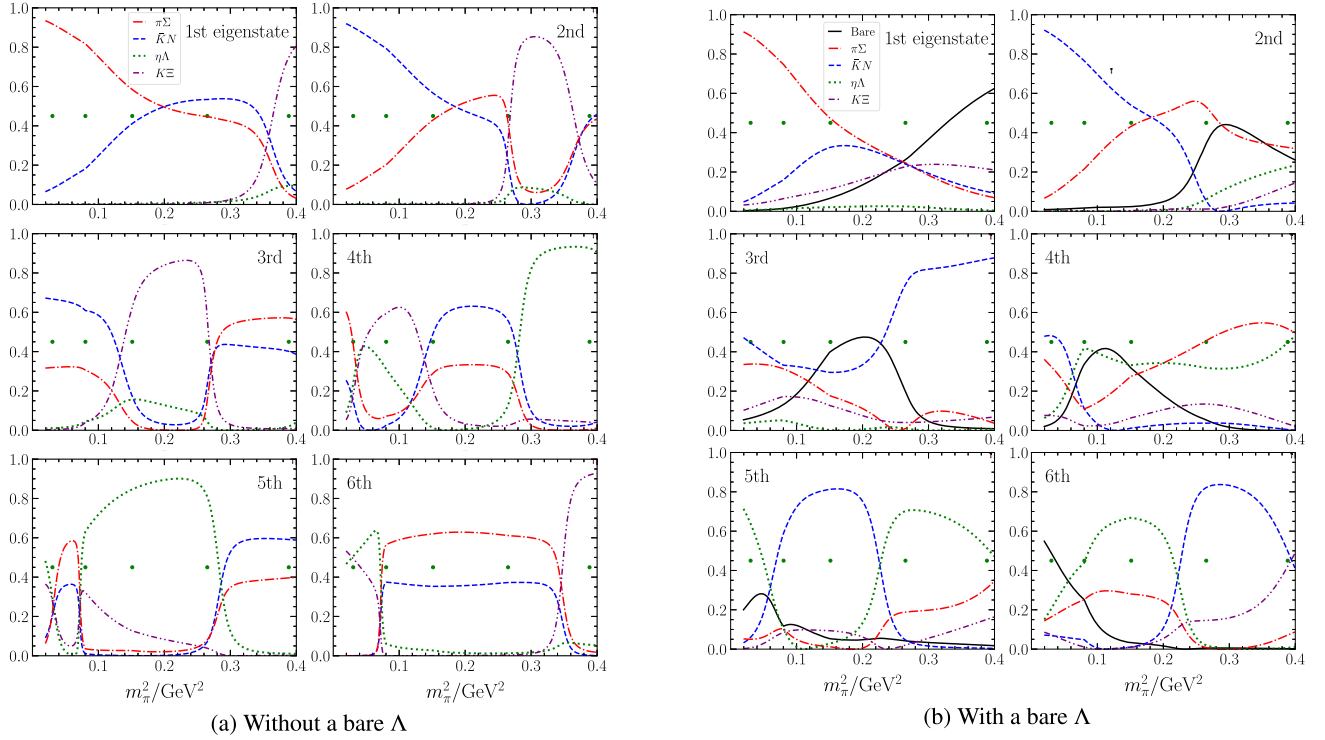


FIG. 3. The pion mass dependence of the Hamiltonian matrix eigenvector components for the first six states, under the assumption of no bare-baryon (left two columns) and including a bare-baryon basis (right two columns). The five circles in each diagram represent the five quark masses considered by the CSSM group [31,38] in 2 + 1 flavor QCD [99].

consistent with the lattice QCD data at small pion masses, but display significant differences for the two heaviest quark masses considered.

We show the corresponding eigenvectors in Fig. 3(a) for this first scenario. Near the physical pion mass, the first and second eigenstates are mainly $\pi\Sigma$ and $\bar{K}N$ states, respectively. The second and third eigenstates are predominantly mixtures of these two channels with $\bar{K}N$ continuing to dominate the third state. The fifth and sixth states are dominated by the $K\Xi$ and $\eta\Lambda$ mixture. The fifth and sixth eigenenergies in the ~ 3 fm box are close to the position of the $\Lambda(1670)$ at the physical pion mass, as we see in Fig. 2(a). With the fourth, fifth and sixth states residing in the region of the $\Lambda(1670)$ resonance, all four of the two-particle channels considered can play an important role in governing the structure of this resonance.

However, at large pion masses, these results without a bare baryon are inconsistent with the lattice QCD data. This was also reported in our earlier work, which focused on the $\Lambda(1405)$ [37]. From Fig. 2(a), the lattice simulation at the largest pion mass is considerably lower than the first Hamiltonian eigenstate. This greatly reduces the probability that the odd-parity Λ spectrum can be described by a model without the bare baryon.

To study the case with a bare quark-model-like baryon, we need to know the variation of the bare mass, m_B^0 , as the pion mass increases. Within the quark model its mass is

expected to increase linearly with the light quark mass as m_π^2 increases and hence we take

$$m_B^0(m_\pi^2) = m_B^0|_{phy} + \alpha_B^0(m_\pi^2 - m_\pi^2|_{phy}). \quad (4.2)$$

For the $N^*(1535)$, $\alpha_N^0 = 0.944 \text{ GeV}^{-1}$ was obtained in Ref. [41]. For the Λ , where the strange quark mass is held fixed, it is natural to take 2/3 of this, such that $\alpha_B^0 = 0.629 \text{ GeV}^{-1}$.

In Fig. 2(b) we present the Λ spectrum with a bare baryon basis state. Our results clearly reproduce the lattice QCD simulations well at all pion masses. The content of the corresponding eigenstates is shown in Fig. 3(b). Some of this information has been brought to Fig. 2(b), where color and texture have been added to the solid lines indicating the eigenstate energies. This additional information illustrates the energy eigenstates where the bare baryon state makes a substantial contribution to the composition of the state in HEFT. The largest bare basis-state contribution is illustrated in solid red, the second largest in dot-dash blue and the third largest in dotted green.

In the first eigenstate, the main component is $\pi\Sigma$ at small pion masses, while the contributions of $\pi\Sigma$ and $\bar{K}N$ channels become comparable and then the bare baryon dominates as the pion mass becomes larger. The second eigenstate is mainly composed of $\bar{K}N$, while the third and

fourth are dominated by the $\bar{K}N$ and $\pi\Sigma$ channels at small pion masses with $\bar{K}N$ continuing to dominate for both states. At the physical pion mass, the fifth state is dominated by $\eta\Lambda$ with a significant bare baryon component. The sixth state is dominated by the quark-model-like basis state. Remarkably, all four of the two-particle channels provide the balance of basis-state contributions at the physical point.

With the bare basis state contributing in the $\Lambda(1670)$ region, it is now clear the CSSM collaboration was able to excite the $\bar{K}N$ state with a local three-quark operator due to its localized structure. While the strange magnetic form factor shows the contribution of a vacuum quark-antiquark pair to create a 5-quark $\bar{K}N$ state [38], the electric form factors describe a localized state. Figure 3 of Ref. [100] shows the strange quark distribution is largely unchanged between the ground-state positive-parity Λ and its first excitation in the $\Lambda(1405)$ region. Similarly, the light-quark distribution grows only slightly from the ground state to the $\bar{K}N$ state in the $\Lambda(1405)$ resonance regime.

In summary, the lattice QCD results favor the scenario in which the $\Lambda(1670)$ contains a bare-baryon component. As the fifth and sixth states in this description contain very significant quark-model-like basis state contributions and because the fourth, fifth and sixth states sit in the $\Lambda(1670)$ resonance regime, as illustrated in Fig. 2(b), one can conclude that the $\Lambda(1670)$ has a quark-model-like core dressed by all four of the meson-baryon channels considered.

C. Uncertainty analysis

To obtain an error estimate on the link between experiment and the finite-volume spectra driven by the embedded Lüscher relation, we draw on the regularization parameter, Λ , to move in the Hamiltonian parameter space and explore alternative mediations between experiment and theory.

As noted in the previous section, the constraints of experiment and lattice QCD are effective in constraining the Hamiltonian parameters, allowing only a small range of variation in Λ . If one forces Λ outside of the range allowed by the experimental data, the fit to the data is spoiled and thus the associated finite-volume energy spectrum becomes incorrect. In a similar manner, the correct description of lattice QCD results places constraints on the variation of parameters.

We commence by changing Λ by 50 MeV from our initial value of 1.0 GeV and refitting the parameters to describe experiment. This small variation is repeated, monitoring the χ^2 per degree of freedom to ensure the experimental data continues to be described in an accurate manner. The finite volume spectrum is then calculated. We compare the results with the CSSM lattice QCD results to ensure a valid description of the lattice QCD constraint.

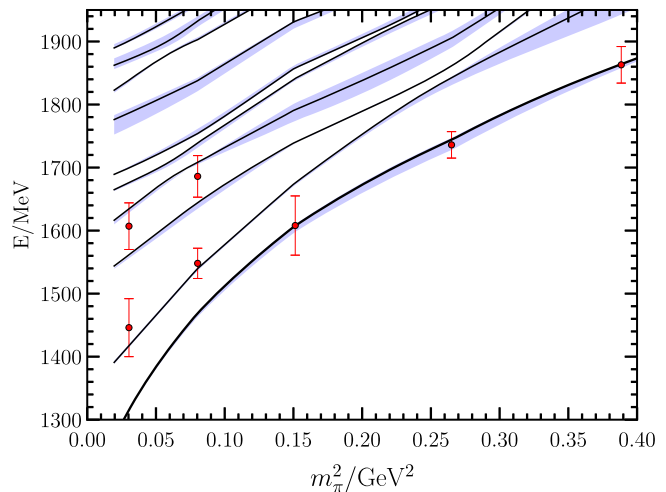


FIG. 4. Error estimation for the spectrum of odd-parity strange spin-1/2 baryons in HEFT for the CSSM lattice volume. The black solid lines represent the values with the optimal Hamiltonian parameters while the blue shaded regions illustrate the uncertainty in the HEFT results obtained through the allowed variation of Hamiltonian parameters as described in Sec. IV C.

The variation of the χ^2/dof for the cross section fits is subtle over the range $0.90 \leq \Lambda \leq 1.10$ GeV but jumps significantly for the values $\Lambda = 0.85$ and 1.15 GeV. On this basis alone, the fits for $\Lambda < 0.85$ GeV and $\Lambda > 1.15$ GeV are excluded. However, considering the lattice QCD constraint further excludes $\Lambda > 1.15$ GeV. Over the range $0.90 \leq \Lambda \leq 1.10$ GeV the three pole positions do not change by more than 10 MeV.

The best description of the lattice QCD results is provided by $\Lambda = 1.00$ GeV and we refer to this for our central values. To produce uncertainties in the finite-volume results, we refer to the predictions for $\Lambda = 0.90$ and 1.10 GeV and use these results to shade error bars in Figs. 4 and 5. Uncertainties in the fit parameters of Table I also follow from this range of allowed Λ variation.

D. Comparison with the latest lattice QCD simulation

One can clearly see that some eigenstates predicted by the HEFT are absent in the lattice QCD simulations of the CSSM group from Fig. 2. More than ten years have passed since that odd-parity Λ spectrum was obtained [31] and lattice QCD techniques have improved. With the parameters of the Hamiltonian constrained by experimental data and the results from one lattice QCD collaboration, we can now proceed to make predictions for the finite-volume spectra observed in other lattice QCD calculations, both at different volumes and at different quark masses. Very recently, the BaSc collaboration presented their coupled-channel simulations with both single baryon and meson-baryon interpolating operators in a larger box at $m_\pi \approx 200$ MeV [62,63]. We now compare our HEFT predictions with this latest lattice QCD simulation.

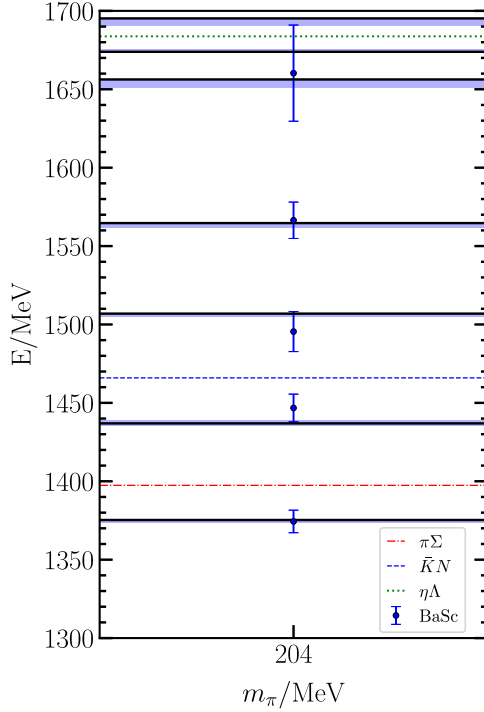


FIG. 5. The energy eigenvalues calculated in HEFT in the scenario including a quark-model-like single-particle basis state (solid black lines) are compared with lattice QCD calculations from the BaSc collaboration [62,63] in the $G_{1u}(0)$ irreducible representation (data points) on a $L = 4.05$ fm lattice. Dashed lines indicate the meson-baryon thresholds. The blue shaded regions illustrate the uncertainty in the HEFT predictions obtained through the allowed variation of Hamiltonian parameters as described in Sec. IV C.

We use the corresponding hadron masses at $m_\pi \sim 200$ MeV as reported in the lattice QCD simulations [62,63] and give our HEFT results, including the bare baryon, in Fig. 5. One can see that the HEFT results describe the BaSc simulations very well. The lowest data point has a very small error bar but sits exactly on our lowest-lying odd-parity state. All of the HEFT energy eigenstates are far from the noninteracting meson-baryon thresholds but still coincide with the lattice results. We stress that no parameters have been adjusted in making the finite volume predictions for the BaSc lattice results.

In our approach, at $m_\pi = 204$ MeV, the first and second states observed in this ~ 4 fm box are mainly $\pi\Sigma$ and $\bar{K}N$ states, respectively. The third and fourth ones are the $\pi\Sigma - \bar{K}N$ mixtures. The fifth eigenstate contains $\bar{K}N$ and $\pi\Sigma$ with some bare baryon. The sixth eigenstate is dominated by $\eta\Lambda$ mixed with a small component of the bare baryon. Noting that the fifth and sixth energy eigenstates are in the $\Lambda(1670)$ resonance regime, one can once again conclude that the $\Lambda(1670)$ is composed of a single-particle quark-model-like core dressed by the isoscalar meson-baryon channels considered.

V. SUMMARY

In this work we have studied two different scenarios for the internal structure of the $\Lambda(1670)$. One scenario assumes that the $\Lambda(1670)$ is dynamically generated through rescattering between the $\bar{K}N$, $\pi\Sigma$, $\eta\Lambda$ and $K\Xi$ channels with $I = 0$. The other assumes that the $\Lambda(1670)$ is a bare quark-model-like basis state mixing with these $I = 0$ interacting channels. We fit the experimental cross section data for the $K^-p \rightarrow K^-p$, $K^-p \rightarrow \bar{K}^0n$, $K^-p \rightarrow \pi^0\Lambda^0$, $K^-p \rightarrow \pi^-\Sigma^+$, $K^-p \rightarrow \pi^0\Sigma^0$, $K^-p \rightarrow \pi^+\Sigma^-$, and $K^-p \rightarrow \eta\Lambda^0$ reactions, with the laboratory momentum of the anti-kaon in the range 0–800 MeV/c, including the recently measured threshold cross sections which have small error bars [60]. Our fits are consistent with the cross section data if we neglect the effect of the D -wave $\Lambda(1520)$ resonance. In addition, we have checked the two-pole structure of the $\Lambda(1405)$ and obtained the pole position of the $\Lambda(1670)$. All of these results are consistent with those of other groups.

It is clear from the quality of the fits to the cross section data under both scenarios that one cannot distinguish between them using scattering data alone. This serves as motivation to introduce HEFT to further explore the structure of the $\Lambda(1670)$ in the finite volume of lattice QCD. The scenario without a bare baryon is inconsistent with the lattice QCD data at large pion masses. Without adjusting any other parameter, the scenario including a bare-baryon basis state yields an excellent description of the lattice QCD results over the full range of light quark mass. Our HEFT results also agree very well with the latest BaSc lattice QCD simulation results at $m_\pi = 204$ MeV. Not only are the predicted energy levels very close to those reported by BaSc, but all five of the lowest eigenstates predicted in HEFT were observed in the lattice calculations.

Based on the present HEFT analysis, the lattice QCD calculations provide invaluable information about the structure of the $\Lambda(1670)$. It definitely contains a considerable single-particle quark-model-like basis state component, which mixes with the meson-baryon channels. While our calculations could be extended by considering the $\Lambda(1800)$ resonance as well as \bar{K}^*N and $\pi\Sigma^*$ channels, the main conclusion in this work is not expected to be sensitive to extensions well beyond the $\Lambda(1670)$ resonance regime.

ACKNOWLEDGMENTS

This work was supported by the National Natural Science Foundation of China under Grants No. 12175091, No. 12335001, No. 12247101, No. 12305090 and No. 12347119, the China National Funds for Distinguished Young Scientists under Grant No. 11825503, National Key Research and Development Program of China under Contract No. 2020YFA0406400, the 111 Project under Grant No. B20063, the innovation project for young science and technology talents of Lanzhou city under Grant

No. 2023-QN-107, the fundamental Research Funds for the Central Universities, and the project for top-notch innovative talents of Gansu province. D.G. is also supported by the China Postdoctoral Science Foundation under Grant No. 2023M740117. This research was undertaken with the assistance of resources from the National Computational Infrastructure (NCI), provided through the National

Computational Merit Allocation Scheme, and supported by the Australian Government through Grant No. LE190100021. This research was supported by the University of Adelaide and by the Australian Research Council through ARC Discovery Project Grants No. DP190102215 and No. DP210103706 (D. B. L.) and No. DP230101791 (A. W. T.).

-
- [1] R. H. Dalitz and S. F. Tuan, The phenomenological description of K^- -nucleon reaction processes, *Ann. Phys. (N.Y.)* **10**, 307 (1960).
- [2] E. Klempt and J. M. Richard, Baryon spectroscopy, *Rev. Mod. Phys.* **82**, 1095 (2010).
- [3] D. Jido, J. A. Oller, E. Oset, A. Ramos, and U. G. Meissner, Chiral dynamics of the two $\Lambda(1405)$ states, *Nucl. Phys.* **A725**, 181 (2003).
- [4] J. A. Oller and U. G. Meissner, Chiral dynamics in the presence of bound states: Kaon nucleon interactions revisited, *Phys. Lett. B* **500**, 263 (2001).
- [5] E. Oset, A. Ramos, and C. Bennhold, Low lying $S = -1$ excited baryons and chiral symmetry, *Phys. Lett. B* **527**, 99 (2002); **530**, 260(E) (2002).
- [6] J. J. Xie and L. S. Geng, The $a_0(980)$ and $\Lambda(1670)$ in the $\Lambda_c^+ \rightarrow \pi^+\eta\Lambda$ decay, *Eur. Phys. J. C* **76**, 496 (2016).
- [7] K. Miyahara, T. Hyodo, and E. Oset, Weak decay of Λ_c^+ for the study of $\Lambda(1405)$ and $\Lambda(1670)$, *Phys. Rev. C* **92**, 055204 (2015).
- [8] R. Pavao, P. Gubler, P. Fernandez-Soler, J. Nieves, M. Oka, and T. T. Takahashi, The negative-parity spin-1/2 Λ baryon spectrum from lattice QCD and effective theory, *Phys. Lett. B* **820**, 136473 (2021).
- [9] S. Capstick and N. Isgur, Baryons in a relativized quark model with chromodynamics, *Phys. Rev. D* **34**, 2809 (1986); *AIP Conf. Proc.* **132**, 267 (1985).
- [10] Y. Chen and B. Q. Ma, Light flavor baryon spectrum with higher order hyperfine interactions, *Nucl. Phys.* **A831**, 1 (2009).
- [11] T. Melde, W. Plessas, and B. Sengl, Quark-model identification of baryon ground and resonant states, *Phys. Rev. D* **77**, 114002 (2008).
- [12] R. Bijker, F. Iachello, and A. Leviatan, Algebraic models of hadron structure. 2. Strange baryons, *Ann. Phys. (N.Y.)* **284**, 89 (2000).
- [13] L. Y. Glozman, W. Plessas, K. Varga, and R. F. Wagenbrunn, Unified description of light and strange baryon spectra, *Phys. Rev. D* **58**, 094030 (1998).
- [14] U. Loring, B. C. Metsch, and H. R. Petry, The light baryon spectrum in a relativistic quark model with instanton induced quark forces: The strange baryon spectrum, *Eur. Phys. J. A* **10**, 447 (2001).
- [15] C. L. Schat, J. L. Goity, and N. N. Scoccola, Masses of the 70- baryons in large N(c) QCD, *Phys. Rev. Lett.* **88**, 102002 (2002).
- [16] G. P. Engel, C. B. Lang, and A. Schäfer (BGR (Bern-Graz-Regensburg) Collaboration), Low-lying Λ baryons from the lattice, *Phys. Rev. D* **87**, 034502 (2013).
- [17] C. S. An, B. Saghai, S. G. Yuan, and J. He, Role of five-quark components in radiative and strong decays of the $\Lambda(1405)$ resonance, *Phys. Rev. C* **81**, 045203 (2010).
- [18] T. Hyodo and D. Jido, The nature of the $\Lambda(1405)$ resonance in chiral dynamics, *Prog. Part. Nucl. Phys.* **67**, 55 (2012).
- [19] J. A. Oller, J. Prades, and M. Verbeni, Surprises in threshold antikaon-nucleon physics, *Phys. Rev. Lett.* **95**, 172502 (2005).
- [20] B. Borasoy, R. Nissler, and W. Weise, Chiral dynamics of kaon-nucleon interactions, revisited, *Eur. Phys. J. A* **25**, 79 (2005).
- [21] T. Hyodo, S. i. Nam, D. Jido, and A. Hosaka, Detailed analysis of the chiral unitary model for meson baryon scatterings with flavor SU(3) breaking effects, *Prog. Theor. Phys.* **112**, 73 (2004).
- [22] C. Garcia-Recio, J. Nieves, E. Ruiz Arriola, and M. J. Vicente Vacas, $S = -1$ meson baryon unitarized coupled channel chiral perturbation theory and the $S(01)$ $\Lambda(1405)$ and $\Lambda(1670)$ resonances, *Phys. Rev. D* **67**, 076009 (2003).
- [23] J. A. Oller, J. Prades, and M. Verbeni, Aspects of strangeness -1 meson-baryon scattering, *Eur. Phys. J. A* **31**, 527 (2007).
- [24] Z. H. Guo and J. A. Oller, Meson-baryon reactions with strangeness -1 within a chiral framework, *Phys. Rev. C* **87**, 035202 (2013).
- [25] H. Zhang, J. Tulpan, M. Shrestha, and D. M. Manley, Partial-wave analysis of $\bar{K}N$ scattering reactions, *Phys. Rev. C* **88**, 035204 (2013).
- [26] H. Zhang, J. Tulpan, M. Shrestha, and D. M. Manley, Multichannel parametrization of $\bar{K}N$ scattering amplitudes and extraction of resonance parameters, *Phys. Rev. C* **88**, 035205 (2013).
- [27] L. S. Geng, E. Oset, and M. Doring, The radiative decay of the $\Lambda(1405)$ and its two-pole structure, *Eur. Phys. J. A* **32**, 201 (2007).
- [28] B. C. Liu and J. J. Xie, $K^-p \rightarrow \eta\Lambda$ reaction in an effective Lagrangian model, *Phys. Rev. C* **85**, 038201 (2012).
- [29] J. J. Xie, B. C. Liu, and C. S. An, Coupling constant for $\Lambda(1405)\bar{K}N$, *Phys. Rev. C* **88**, 015203 (2013).
- [30] C. Garcia-Recio, M. F. M. Lutz, and J. Nieves, Quark mass dependence of s wave baryon resonances, *Phys. Lett. B* **582**, 49 (2004).

- [31] B. J. Menadue, W. Kamleh, D. B. Leinweber, and M. S. Mahbub, Isolating the $\Lambda(1405)$ in lattice QCD, *Phys. Rev. Lett.* **108**, 112001 (2012).
- [32] A. Martinez Torres, M. Bayar, D. Jido, and E. Oset, Strategy to find the two $\Lambda(1405)$ states from lattice QCD simulations, *Phys. Rev. C* **86**, 055201 (2012).
- [33] F. K. Guo, Y. Kamiya, M. Mai, and U. G. Meißner, New insights into the nature of the $\Lambda(1380)$ and $\Lambda(1405)$ resonances away from the SU(3) limit, *Phys. Lett. B* **846**, 138264 (2023).
- [34] E. A. Veit, B. K. Jennings, A. W. Thomas, and R. C. Barrett, S wave meson—nucleon scattering in an SU(3) cloudy bag model, *Phys. Rev. D* **31**, 1033 (1985).
- [35] J. A. Oller, Coupled-channel approach in hadron–hadron scattering, *Prog. Part. Nucl. Phys.* **110**, 103728 (2020).
- [36] J. M. M. Hall, W. Kamleh, D. B. Leinweber, B. J. Menadue, B. J. Owen, and A. W. Thomas, Light-quark contributions to the magnetic form factor of the $\Lambda(1405)$, *Phys. Rev. D* **95**, 054510 (2017).
- [37] Z. W. Liu, J. M. M. Hall, D. B. Leinweber, A. W. Thomas, and J. J. Wu, Structure of the $\Lambda(1405)$ from Hamiltonian effective field theory, *Phys. Rev. D* **95**, 014506 (2017).
- [38] J. M. M. Hall, W. Kamleh, D. B. Leinweber, B. J. Menadue, B. J. Owen, A. W. Thomas, and R. D. Young, Lattice QCD evidence that the $\Lambda(1405)$ resonance is an antikaon-nucleon molecule, *Phys. Rev. Lett.* **114**, 132002 (2015).
- [39] J. J. Wu, T. S. H. Lee, A. W. Thomas, and R. D. Young, Finite-volume Hamiltonian method for coupled-channels interactions in lattice QCD, *Phys. Rev. C* **90**, 055206 (2014).
- [40] Z. W. Liu, W. Kamleh, D. B. Leinweber, F. M. Stokes, A. W. Thomas, and J. J. Wu, Hamiltonian effective field theory study of the $N^*(1535)$ resonance in lattice QCD, *Phys. Rev. Lett.* **116**, 082004 (2016).
- [41] C. D. Abell, D. B. Leinweber, Z. W. Liu, A. W. Thomas, and J. J. Wu, Low-lying odd-parity nucleon resonances as quark-model-like states, *Phys. Rev. D* **108**, 094519 (2023).
- [42] J. M. M. Hall, A. C.-P. Hsu, D. B. Leinweber, A. W. Thomas, and R. D. Young, Finite-volume matrix Hamiltonian model for a $\Delta \rightarrow N\pi$ system, *Phys. Rev. D* **87**, 094510 (2013).
- [43] D. Leinweber *et al.*, N^* spectroscopy from lattice QCD: The Roper explained, *J. Phys. Soc. Jpn. Conf. Proc.* **10**, 010011 (2016).
- [44] K. Yu, Y. Li, J. J. Wu, D. B. Leinweber, and A. W. Thomas, Study of the pion-mass dependence of ρ -meson properties in lattice QCD, *Phys. Rev. D* **109**, 034505 (2024).
- [45] M. Mai, Review of the $\Lambda(1405)$ A curious case of a strangeness resonance, *Eur. Phys. J. Special Topics* **230**, 1593 (2021).
- [46] T. Hyodo and M. Niyama, QCD and the strange baryon spectrum, *Prog. Part. Nucl. Phys.* **120**, 103868 (2021).
- [47] U. G. Meißner, Two-pole structures in QCD: Facts, not fantasy!, *Symmetry* **12**, 981 (2020).
- [48] J. M. Xie, J. X. Lu, L. S. Geng, and B. S. Zou, Two-pole structures as a universal phenomenon dictated by coupled-channel chiral dynamics, *Phys. Rev. D* **108**, L111502 (2023).
- [49] J. X. Lu, L. S. Geng, M. Doering, and M. Mai, Cross-channel constraints on resonant antikaon-nucleon scattering, *Phys. Rev. Lett.* **130**, 071902 (2023).
- [50] Z. Y. Wang, J. J. Qi, J. Xu, and X. H. Guo, Analyzing $\Xi(1620)$ in the molecule picture in the Bethe-Salpeter equation approach, *Eur. Phys. J. C* **79**, 640 (2019).
- [51] K. Chen, R. Chen, Z. F. Sun, and X. Liu, $\bar{K}\Lambda$ molecular explanation to the newly observed $\Xi(1620)^0$, *Phys. Rev. D* **100**, 074006 (2019).
- [52] M. Sumihama *et al.* (Belle Collaboration), Observation of $\Xi(1620)^0$ and evidence for $\Xi(1690)^0$ in $\Xi_c^+ \rightarrow \Xi^- \pi^+ \pi^+$ decays, *Phys. Rev. Lett.* **122**, 072501 (2019).
- [53] R. Aaij *et al.* (LHCb Collaboration), Observation of $J/\psi p$ resonances consistent with pentaquark states in $\Lambda_b^0 \rightarrow J/\psi K^- p$ decays, *Phys. Rev. Lett.* **115**, 072001 (2015).
- [54] R. Aaij *et al.* (LHCb Collaboration), Observation of a narrow pentaquark state, $P_c(4312)^+$, and of two-peak structure of the $P_c(4450)^+$, *Phys. Rev. Lett.* **122**, 222001 (2019).
- [55] R. Aaij *et al.* (LHCb Collaboration), Study of the doubly charmed tetraquark T_{cc}^+ , *Nat. Commun.* **13**, 3351 (2022).
- [56] R. Aaij *et al.* (LHCb Collaboration), Observation of an exotic narrow doubly charmed tetraquark, *Nat. Phys.* **18**, 751 (2022).
- [57] R. Aaij *et al.* (LHCb Collaboration), Evidence of a $J/\psi\Lambda$ structure and observation of excited Ξ^- states in the $\Xi_b^- \rightarrow J/\psi\Lambda K^-$ decay, *Sci. Bull.* **66**, 1278 (2021).
- [58] R. Aaij *et al.* (LHCb Collaboration), Observation of a $J/\psi\Lambda$ resonance consistent with a strange pentaquark candidate in $B^- \rightarrow J/\psi\Lambda p^-$ decays, *Phys. Rev. Lett.* **131**, 031901 (2023).
- [59] J. j. Wu, D. B. Leinweber, Z. w. Liu, and A. W. Thomas, Structure of the Roper resonance from lattice QCD constraints, *Phys. Rev. D* **97**, 094509 (2018).
- [60] K. Piscicchia, M. Skurzok, M. Cargnelli, R. Del Grande, L. Fabbietti, J. Marton, P. Moskal, A. Ramos, A. Scordo, D. L. Sirghi *et al.*, First simultaneous $K^- p \rightarrow \Sigma^0 \pi^0$, $\Lambda \pi^0$ cross section measurements at 98 MeV/c, *Phys. Rev. C* **108**, 055201 (2023).
- [61] P. Gubler, T. T. Takahashi, and M. Oka, Flavor structure of Λ baryons from lattice QCD: From strange to charm quarks, *Phys. Rev. D* **94**, 114518 (2016).
- [62] J. Bulava *et al.* (Baryon Scattering (BaSc) Collaboration), Lattice QCD study of $\pi\Sigma - \bar{K}N$ scattering and the $\Lambda(1405)$ resonance, *Phys. Rev. D* **109**, 014511 (2024).
- [63] J. Bulava *et al.* (Baryon Scattering (BaSc) Collaboration), The two-pole nature of the $\Lambda(1405)$ from lattice QCD, *Phys. Rev. Lett.* **132**, 051901 (2024).
- [64] S. Aikawa *et al.* (J-PARC E31 Collaboration), Pole position of $\Lambda(1405)$ measured in $d(K^-, n)\pi\Sigma$ reactions *Phys. Lett. B* **837**, 137637 (2023).
- [65] S. Acharya *et al.* (ALICE Collaboration), Kaon–proton strong interaction at low relative momentum via femtoscopy in Pb–Pb collisions at the LHC, *Phys. Lett. B* **822**, 136708 (2021).
- [66] J. Zmeskal, M. Sato, S. Ajimura, M. Bazzi, G. Beer, C. Berucci, H. Bhang, D. Bosnar, M. Bragadireanu, P. Buehler *et al.*, Measurement of the strong interaction induced shift and width of the $1s$ state of kaonic deuterium at J-PARC, *Acta Phys. Pol. B* **46**, 101 (2015).

- [67] M. Bazzi *et al.* (SIDDHARTA Collaboration), A new measurement of kaonic hydrogen x-rays, *Phys. Lett. B* **704**, 113 (2011).
- [68] A. W. Thomas, Chiral symmetry and the bag model: A new starting point for nuclear physics, *Adv. Nucl. Phys.* **13**, 1 (1984).
- [69] S. Weinberg, Pion scattering lengths, *Phys. Rev. Lett.* **17**, 616 (1966).
- [70] A. W. Thomas, Low-energy pion scattering in the cloudy bag model, *J. Phys. G* **7**, L283 (1981).
- [71] C. D. Abell, D. B. Leinweber, A. W. Thomas, and J. J. Wu, Regularization in nonperturbative extensions of effective field theory, *Phys. Rev. D* **106**, 034506 (2022).
- [72] C. Morningstar, J. Bulava, A. D. Hanlon, B. Hörz, D. Mohler, A. Nicholson, S. Skinner, and A. Walker-Loud, Progress on meson-baryon scattering, *Proc. Sci. LATTICE2021* (2022) 170.
- [73] C. B. Lang, L. Leskovec, M. Padmanath, and S. Prelovsek, Pion-nucleon scattering in the Roper channel from lattice QCD, *Phys. Rev. D* **95**, 014510 (2017).
- [74] J. Bulava, A. D. Hanlon, B. Hörz, C. Morningstar, A. Nicholson, F. Romero-López, S. Skinner, P. Vranas, and A. Walker-Loud, Elastic nucleon-pion scattering at $m\pi = 200$ MeV from lattice QCD, *Nucl. Phys. B* **987**, 116105 (2023).
- [75] R. G. Edwards, J. J. Dudek, D. G. Richards, and S. J. Wallace, Excited state baryon spectroscopy from lattice QCD, *Phys. Rev. D* **84**, 074508 (2011).
- [76] R. G. Edwards *et al.* (Hadron Spectrum Collaboration), Flavor structure of the excited baryon spectra from lattice QCD, *Phys. Rev. D* **87**, 054506 (2013).
- [77] C. B. Lang and V. Verduci, Scattering in the πN negative parity channel in lattice QCD, *Phys. Rev. D* **87**, 054502 (2013).
- [78] P. Nordin, S- and P-wave interactions of K- mesons in hydrogen, *Phys. Rev.* **123**, 2168 (1961).
- [79] D. Berley, S. P. Yamin, R. R. Kofler, A. Mann, G. W. Meisner, S. S. Yamamoto, J. Thompson, and W. Willis, K^-p amplitudes near the $\Lambda(1520)$, *Phys. Rev. D* **1**, 1996 (1970); **3**, 2297(E) (1971).
- [80] M. Ferro-Luzzi, R. D. Tripp, and M. B. Watson, Excited hyperon of mass 1520 MeV, *Phys. Rev. Lett.* **8**, 28 (1962).
- [81] M. B. Watson, M. Ferro-Luzzi, and R. D. Tripp, Analysis of Y_0^* (1520) and determination of the sigma parity, *Phys. Rev.* **131**, 2248 (1963).
- [82] P. Eberhard, A. H. Rosenfeld, F. T. Solmitz, R. D. Tripp, and M. B. Watson, K-hydrogen charge-exchange scattering, *Phys. Rev. Lett.* **2**, 312 (1959).
- [83] J. Ciborowski *et al.*, Kaon scattering and charged sigma hyperon production in K^-P interactions below 300-MeV/c, *J. Phys. G* **8**, 13 (1982).
- [84] G. S. Abrams and B. Sechi-Zorn, Charge-exchange scattering of low-energy K- mesons in hydrogen, *Phys. Rev.* **139**, B454 (1965).
- [85] M. Sakitt, T. B. Day, R. G. Glasser, N. Seeman, J. H. Friedman, W. E. Humphrey, and R. R. Ross, Low-energy K- meson interactions in hydrogen, *Phys. Rev.* **139**, B719 (1965).
- [86] D. Evans, J. V. Major, E. Rondio, J. A. Zakrzewski, J. E. Conboy, D. J. Miller, and T. Tymieniecka, Charge exchange scattering in K^-P interactions below 300-MeV/c, *J. Phys. G* **9**, 885 (1983).
- [87] T. S. Mast, M. Alston-Garnjost, R. O. Bangerter, A. S. Barbaro-Galtieri, F. T. Solmitz, and R. D. Tripp, The reactions $K^-p \rightarrow \Sigma^0\pi^0$ and $K^-p \rightarrow \Lambda\pi^0$ in the momentum range 240-MeV/c to 450-MeV/c, *Phys. Rev. D* **11**, 3078 (1975).
- [88] J. K. Kim, Low energy K^-p interaction of the 1405 MeV Y_0^* resonance as $\bar{K}N$ bound state, *Phys. Rev. Lett.* **14**, 29 (1965).
- [89] T. S. Mast, M. Alston-Garnjost, R. O. Bangerter, A. S. Barbaro-Galtieri, F. T. Solmitz, and R. D. Tripp, Elastic, charge exchange, and total K^-p cross-sections in the momentum range 220-MeV/c to 470-MeV/c, *Phys. Rev. D* **14**, 13 (1976).
- [90] R. O. Bangerter, M. Alston-Garnjost, A. Barbaro-Galtieri, T. S. Mast, F. T. Solmitz, and R. D. Tripp, Reactions $K^-p \rightarrow \Sigma^-\pi^+$ and $K^-p \rightarrow \Sigma^+\pi^-$ in the momentum range from 220-MeV/c to 470-MeV/c, *Phys. Rev. D* **23**, 1484 (1981).
- [91] M. F. M. Lutz and E. E. Kolomeitsev, Relativistic chiral SU(3) symmetry, large N(c) sum rules and meson baryon scattering, *Nucl. Phys. A* **700**, 193 (2002).
- [92] G. I. He and R. H. Landau, A cloudy bag model for the S—D wave anti-K—N system, *Phys. Rev. C* **48**, 3047 (1993).
- [93] X. H. Zhong and Q. Zhao, Low energy reactions $K^-p \rightarrow \Sigma^0\pi^0$, $\Lambda\pi^0$, \bar{K}^0n and the strangeness $S = -1$ hyperons, *Phys. Rev. C* **88**, 015208 (2013).
- [94] X. H. Zhong and Q. Zhao, The $K^-p \rightarrow \pi^0\Sigma^0$ reaction at low energies in a chiral quark model, *Phys. Rev. C* **79**, 045202 (2009).
- [95] A. V. Sarantsev, M. Matveev, V. A. Nikonov, A. V. Anisovich, U. Thoma, and E. Klempt, Hyperon II: Properties of excited hyperons, *Eur. Phys. J. A* **55**, 180 (2019).
- [96] H. Kamano, S. X. Nakamura, T. S. H. Lee, and T. Sato, Dynamical coupled-channels model of K^-p reactions. II. Extraction of Λ^* and Σ^* hyperon resonances, *Phys. Rev. C* **92**, 025205 (2015); **95**, 049903(E) (2017).
- [97] C. Garcia-Recio, J. Nieves, E. Ruiz Arriola, and M. J. Vicente Vacas, S = -1 meson baryon unitarized coupled channel chiral perturbation theory and the S(01) $\Lambda(1405)$ and $\Lambda(1670)$ resonances, *Phys. Rev. D* **67**, 076009 (2003).
- [98] J. j. Wu *et al.*, Nucleon excited states from lattice QCD and Hamiltonian effective field theory, arXiv:1805.05066.
- [99] S. Aoki *et al.* (PACS-CS Collaboration), 2 + 1 flavor lattice QCD toward the physical point, *Phys. Rev. D* **79**, 034503 (2009).
- [100] B. J. Menadue, W. Kamleh, D. B. Leinweber, M. Selim Mahbub, and B. J. Owen, Electromagnetic form factors for the $\Lambda(1405)$, *Proc. Sci. LATTICE2013* (2014) 280.